SCIENCE CHINA
Technological Sciences

Special Topic: High-speed Railway Infrastructure (II)
• Article •

February 2015 Vol.58 No.2: 236–247
doi: 10.1007/s11431-014-5750-7

Vertical dynamic response of the ballastless track on long-span plate-truss cable-stayed bridges

LI YongLe[1,3*], SU Yang[1], XIA FeiLong[1] & ZHANG Nan[2]

[1] *Department of Bridge Engineering, Southwest Jiaotong University, Chengdu 610031, China;*
[2] *Department of Bridge Engineering, Northern Jiaotong University, Beijing 100044, China;*
[3] *MOE Key Laboratory of High Speed Railway Engineering, Southwest Jiaotong University, Chengdu 610031, China*

Received September 23, 2014; accepted December 11, 2014

An analytical model is presented to study vertical dynamic response of the ballastless track on long-span plate-truss cable-stayed bridges based on an explicit dynamic analysis method. In the model, the train, ballastless track and bridge are treated as a coupled vibration system with interaction. By simulating the dynamic process of the system, this paper discusses the distribution law of dynamic responses of the bridge deck and the bed slab. It shows the necessity of a base plate for the ballastless track on the long-span plate-truss cable-stayed bridge. Comparison of the influence of different train speeds and stiffness of the elastic vibration-damping pad on the dynamic responses of the bridge deck and the bed slab is also made. The reasonable stiffness value of elastic vibration-damping pad is proposed.

long-span cable-stayed bridge, plate-truss girder, ballastless track, train-induced vibration, vehicle-bridge system

Citation: Li Y L, Su Y, Xia F L, et al. Vertical dynamic response of the ballastless track on long-span plate-truss cable-stayed bridges. Sci China Tech Sci, 2015, 58: 236–247, doi: 10.1007/s11431-014-5750-7

1 Introduction

The ballastless track structure is becoming a development direction of the high-speed railway track structure because of its less maintenance workload, better durability and smaller plastic deformation compared with other track structures. Meanwhile, the long-span plate truss cable- stayed bridge, with sufficient lateral and vertical stiffness to meet the requirements of high-speed trains, becomes an appropriate structure form for a long-span railway bridge. Laying the ballastless track on the long-span plate truss cable-stayed bridge is an effective way to extend the maintenance cycle of the track structure, improve the efficiency and smoothness of the track, and reduce the dead loads on the bridge, as well save construction costs [1].

However, the elasticity of ballastless track is poor. The vibration of track structure and bridge structure will be intensified with the train axle loads. And the uneven stiffness of long-span plate truss cable-stayed bridge can cause larger vibration under high-speed train loads. As the matter of fact, it is necessary to integrate the train, ballastless track and bridge into an interactive system for further analysis [2,3].

Train-track-bridge interaction is a classic railway dynamic topic that has been studied for quite some time. During the last two decades, much attention had been paid to bridges, focusing on the analytical low-frequency vibration responses of bridge and the key factors contributing to train-bridge system resonance [4–6]. As the operating train speed steadily increases, great attention was paid to this topic [2]. Arvidsson and Karoumi [7] reviewed the field of train-bridge interaction and discussed the most influential system parameters. In the paper, the research on train-bridge

*Corresponding author (email: lele@swjtu.edu.cn)

interaction, bridge-track interaction, wheel-rail contact, etc and other key model parameters were summarized. Zhai and Cai [8,9] established a vertical train-track-bridge dynamic interaction model to evaluate the vertical dynamic performance of bridge with slab track structure. Cheng et al. [10] proposed a new element called bridge-track-vehicle element to investigate the interactions among a moving train, its supporting railway track structure and bridge structure. The investigation shows that the effect of track structure on the dynamic response of bridge structure is insignificant. The effect of the bridge structure on the dynamic response of the track structure is considerable. Zhang et al. [11] proposed a vehicle-track-bridge dynamic analysis method to study the Evaluation of a vehicle-track-bridge interacted system for the continuous CRTS-II non-ballast track slab. In the method, the vehicle subsystem equations are established by the rigid body dynamics method, the track subsystem and the bridge subsystem equations are established by the FEM. Biondi et al. [12] presented a substructure approach for analyzing the vibration of railway bridges under moving trains with consideration of track structure. Both the rails and bridge were modeled as Bernoulli-Euler beams, while the ballast was characterized as a viscoelastic foundation in the paper. Zhu et al. [13] established a vertical coupled dynamic model of a vehicle and the CRTS I slab track to investigate the damage evolution and the dynamic response of the cement asphalt mortar layer when the vehicle moves along the slab track. Lou et al. [14] proposed a rail-bridge coupling element of unequal lengths, based on the obvious difference of flexural rigidity between rail and bridge.

Most of the cited research works only involved the 2D train-track-bridge interaction. The research on the three-dimensional (3D) train-track-bridge interaction has been reported less. Wu et al. [15] developed a vehicle-rail-bridge interaction model for analyzing the 3D dynamic interaction between trains and railway bridges. In the analysis, three types of vehicle-rail interaction elements were derived. Guo et al. [16] established a 3D dynamic analysis model for a coupled train-bridge system. And the vehicle subsystem was modeled by multibody dynamics. For the bridge subsystem, a 3D rail-ballast-beam finite element model was created with consideration of elasticity and continuity of the track system.

However, early works generally had been directed towards overall vibration of the train-track-bridge system. And most of the researches concentrated on the medium- and small-span railway bridges. Besides, the ballastless track structure was not treated as the research emphasis. The understanding of local vibration performance of ballastless track on a long-span plate-truss cable-stayed bridge was relatively limited. Due to the low vibration frequency of the long-span bridge, the overall vibration acceleration of bridge deck is relatively small. Instead, it is more likely to induce the local vibration. Due to the deformation and the interaction between track and bridge, there is no precedent for laying ballastless track on the long-span plate truss cable-stayed bridge at home and abroad. The related technical parameters and design requirements for a long-span steel beam laying the ballastless track are lack of references. And local vibration of the bridge floor system and the ballastless track caused by the train are lack of awareness. Therefore, it is still significant to carry out research for the vertical dynamic response of the ballastless track on long-span plate-truss cable-stayed bridges.

In the present study, a long-span plate truss cable-stayed bridge laying the double-block ballastless track is introduced as an engineering example. By using the LS-DYNA, the local vibration model in the vertical direction is used to analyze the distribution law and characteristics of local vibration of the bed slab and the bridge deck within the internodes. The model is also used to study the necessity of setting up a base plate for the ballastless track and compare the influence of different train speeds on the dynamic responses of the bridge deck and bed slab. Finally, optimization about the stiffness of the elastic vibration-damping pad is proposed.

2 Analysis model

2.1 Track structure

CRTS I double-block ballastless track consists of rail, elastic fastener, double-block sleeper, bed slab and base slab, as shown in Figure 1. Due to the hierarchical design of double-block ballastless track, the force acting on it is clear. The elastic vibration-damping pad of the track structure has a certain effect of vibration reduction. The double-block ballastless track is easy to accommodate the deformation of steel beam. Thus, it is more reasonable to lay a CRTS I double-block ballastless track on the railway bridge. Both the bed slab and base plate are modeled by the Hughes-Liu shell elements. There are two integration points along the element thickness direction. The rail is modeled by the Hughes-Liu beam elements, using 2×2 Gauss unit integral criterion. Fasteners and elastic vibration-damping pads are modeled by the explicit discrete beam element to describe its vertical stiffness and damping. The ballastless track calculation parameters are shown in Table 1.

2.2 Bridge structure

The cable-stayed bridge with steel truss girder is shown in Figure 2. It has five spans with a total length of 1290 m (90+240+630+240+90 m). The upper deck is designed as 6-lane highway, and the lower deck is designed as quadruple line railway. The steel truss girder is designed as the N-shaped truss with the whole width of 34.2 m and the height of 15.5 m. Each section length is 15 m.

The whole vertical stiffness of the bridge and running

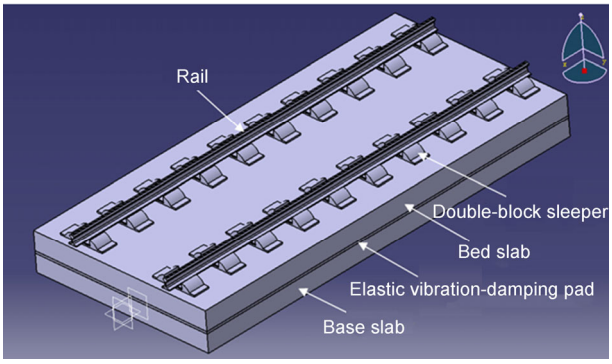

Figure 1 (Color online) Double-block ballastless track.

Table1 Calculation parameters of double-block ballastless track

Component	Category	Parameters
Rail	Type	CHN60
	Height	176 mm
Fastener	Type	WJ-8B
	Height	34 mm
	Spacing	600 mm
	Dynamic stiffness	50 kN/mm
Bed slab	Material	C40 concrete
	Dimension	5900 mm×2800 mm×260 mm
Elastic vibration-damping pad	Stuffiness	0.05 N/mm^3
	Dimension	5900 mm×2800 mm×30 mm
Base slab	Material	C40 concrete
	Dimension	5900 mm×2800 mm×240 mm
Groove	Dimension	1000 mm×700 mm×100 mm

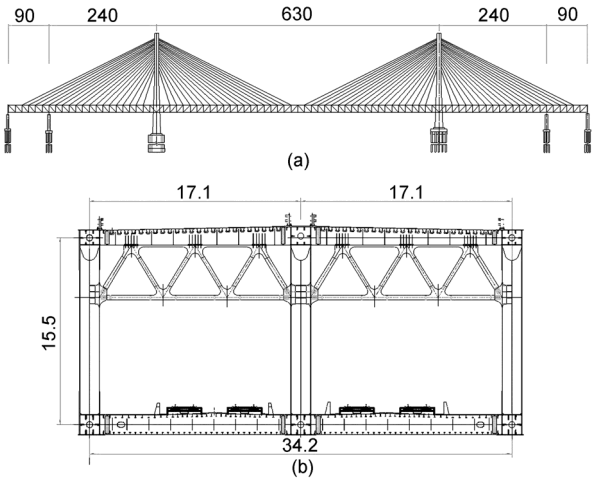

Figure 2 Bridge structure (unit: m). (a) Elevation drawing of the truss; (b) cross section of the truss.

performance of trains meet the design requirements. In order to fully consider local stress behavior of the ballastless track laid on the railway bridge deck, six internodes with weaker stiffness in the middle span are selected as the research objects. The local refinement model of the six internodes are shown in Figure 3, with two internodes on each side called boundary internodes which are used to simulate boundary conditions and two internodes in the middle for analysis called calculation internodes.

Since the main consideration is the local vibration of the railway bridge floor system, only the shell model of railway bridge floor system and bottom chord are established in the explicit dynamics calculation to reduce the number of elements. The lateral-, vertical- and longitudinal-displacement of both ends of the bottom chord are restricted. And the vertical displacement of the connection between bottom chords and webs is restricted. The geometric parameters of the bridge floor system are shown in Table 2.

2.3 Vertical vibration model of ballastless track

The ballastless track on the long-span plate-truss cable-stayed bridge can be excited by the running train to vibrate vertically. It is difficult to simulate this dynamic behavior. The calculation model is very complicated, even impossible to be established. Therefore, it is necessary to employ some proper simplification to achieve the research target and improve the calculation efficiency as well as reliability. For the vertical vibration model of ballastless track on the long-span plate-truss cable-stayed bridge, the following assumptions are made.

(1) The train is simplified into a multi-rigid-body system which consists of a car body, two bogies and four wheel sets. Various parts of the trains are reduced to geometric center of the rigid body neglecting the lateral vibration of each part. The model is shown in Figure 4. The car body, bogies and wheel sets are simulated by rigid body elements. The secondary spring and secondary vertical damping between the bogie and car body as well as the primary spring and primary vertical damping between the wheel set and bogie are stimulated by the explicit discrete beam elements. Basic parameters of the train are shown in Table 3.

(2) As to the calculation of wheel–rail contact forces, lit-

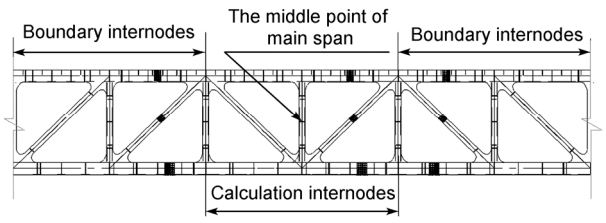

Figure 3 Schematic diagram of internodes.

Table 2 Geometric parameters of bridge floor system

Component	Plate thickness (mm)
Bridge deck	16
U-rib	8
Crossbeam web	16
Lower flange of crossbeam	40
Longitudinal Beam	12
Vertical stiffener of crossbeam	10
Longitudinal stiffener of bridge deck	20

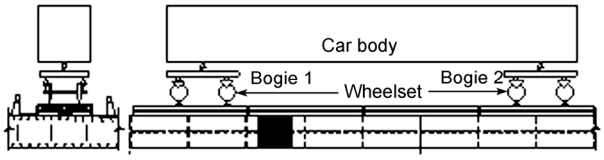

Figure 4 Vertical vibration model of train-ballastless track- bridge system.

Table 3 Basic parameters of train

Parameter name	CRH2	ICE3
Wheel radius (m)	0.43	0.46
Body mass (kg)	39600	48000
Nod moment of inertia of the body (kg m^2)	1940000	2700000
Bogie mass (kg)	3500	3200
Nod moment of inertia of the bogie (kg m^2)	1752	7200
Wheel mass (kg)	2000	2400
Primary vertical stiffness (kN/m)	1176	1040
Primary vertical damping (kN s/m)	19.6	30
Secondary vertical stiffness (kN/m)	196	400
Secondary vertical damping (kN s/m)	40	33.3
Running speeds (km/h)	200–300	300–400

erature [17] recommends a linear wheel-rail contact stiffness values at 2.0×10^9 N/m. There are also some literatures picking the wheel-rail contact stiffness of 1.6×10^9 N/m. In the present study, the non-linear Hertzian elastic contact theory is used to calculate the wheel-rail normal contact forces based on literature [2,3].

$$p(t)=\left[\frac{1}{G}\delta Z(t)\right]^{3/2}, \tag{1}$$

where G is the wheel-rail contact constant; $\delta Z(t)$ is the wheel-rail normal elastic compression deformation.

For the wheel-rail normal elastic compression deformation:

$$\delta Z(t)=Gp(t)^{2/3}. \tag{2}$$

For the wheel-rail contact nonlinear stiffness:

$$K_c=\frac{\mathrm{d}p(t)}{\mathrm{d}\delta Z(t)}. \tag{3}$$

The static compression amount δ_0 under the action of static wheel load P_0 can be used as a reference to the equivalent linear stiffness of the wheel-rail contact K_h. The dynamic compression amount under the action of dynamic wheel load p_1 can be treated as the upper limit to the K_h. According to the Hooke law, the equivalent linear contact stiffness is

$$K_h=\frac{\Delta p(t)}{\Delta\delta Z(t)}=\frac{p_1-p_0}{\delta_1-\delta_0}. \tag{4}$$

The equivalent linear contact stiffness is obtained according to put eq. (2) into eq. (4):

$$K_h=\frac{\Delta p(t)}{\Delta\delta Z(t)}=\frac{p_1-p_0}{G(P_1^{2/3}-P_0^{2/3})}. \tag{5}$$

Ref. [18] suggests that the dynamic wheel load generally takes p_1=1.45p_0.

According to ref. [19], wheel-rail contact constant for the tapered tread surface can be calculated by

$$G=4.57R^{-0.149}\times10^{-8}(\mathrm{m/N^{2/3}}), \tag{6}$$

where R is the train wheel radius.

According to the above formulas, we can get the equivalent linear contact stiffness of CRH2 and ICE3 trains, the results are shown in Table 4.

(3) Getting the sample space of track irregularity by calculating German low disturb spectrum，the power spectral density function is as follows.

Vertical irregularity:

$$S_v(\Omega)=\frac{A_v\Omega_c^2}{(\Omega^2+\Omega_r^2)(\Omega^2+\Omega_c^2)}. \tag{7}$$

The parameters are shown in Table 5.

Track irregularity can be approximately considered as a zero mean Gaussian process. A 1000 m vertical irregularity sample is simulated through the trigonometric series method which is introduced in ref. [20]. The German low disturb spectrum with wavelength from 0.3 to 100 m is adopted as track irregularity in the case study, shown in Figure 5.

Simplified dynamic model of the ballastless track on the long-span plate-truss cable-stayed bridge is shown in Figure 6.

2.4 Stable time setting

At the initial moment of the calculation, the train and the bridge are two independent subsystems and there is no contact force between the wheel-rail. After the gravitational acceleration is added on, there will be contact force between the wheel and the rail. But at this moment, the train load is a very large impact load which will cause the bridge structure and the track structure to vibrate violently. It is inconsistent with the actual situation for a train running on the bridge.

Table 4 Wheel-rail equivalent contact stiffness

Train	Static wheel load (kN)	Dynamic wheel load (kN)	Wheel radius (m)	Wheel-rail contact constant (m/N$^{2/3}$)	Equivalent contact stiffness (N/m)
CRH2	6.695×10^4	9.708×10^4	4.300×10^{-1}	5.182×10^{-8}	1.254×10^9
ICE3	7.848×10^4	1.138×10^5	4.600×10^{-1}	5.131×10^{-8}	1.336×10^9

Table 5 Parameters of German track spectrum

Track level	Ω_c (rad/m)	Ω_r (rad/m)	A_v ($\times10^{-7}$ m rad)
Low interference	0.8246	0.0206	4.032

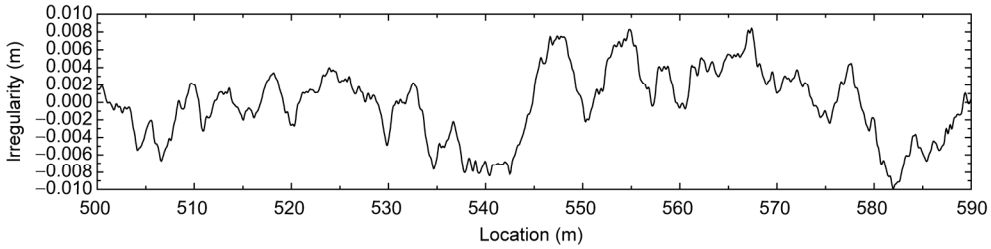

Figure 5 Vertical irregularity samples.

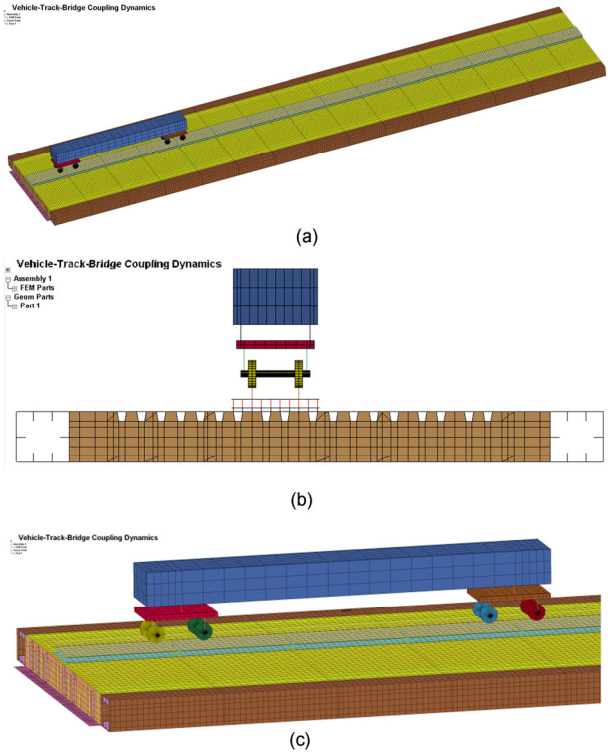

Figure 6 (Color online) Dynamic model of ballastless track on the plate truss cable-stayed bridge. (a) Overall graph of the model; (b) side view; (c) local graph of train.

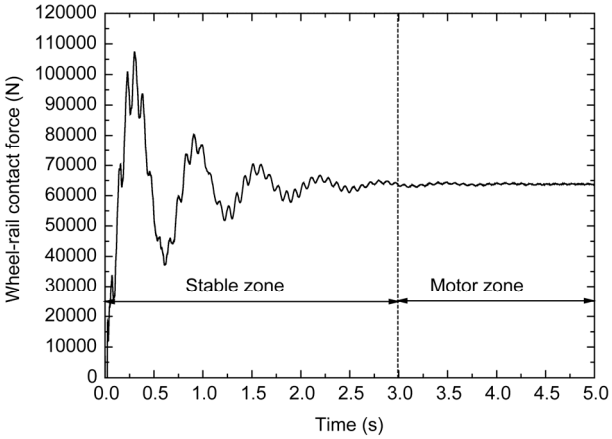

Figure 7 Time history of wheel-rail contact force.

Aiming at this problem, a certain length of subgrade line is set on the end of the bridge according to ref. [21]. This line includes start zone, loading zone, stable zone and excessive zone.

In order to reduce the element number and save calculation costs, steady state vibration of the bed slab and the bridge deck has been obtained. Figure 7 is the time history of wheel-rail contact force. As the figure shows, the wheel-rail contact force and dynamic responses of the bed slab and the base plate decay to the stable value after 3 s. To make sure that the dynamic responses of the track structure and the bridge structure under the action of train loads are fully attenuated, the entire time period is divided into two parts in the follow-up calculation. It is shown that 0–3 s is the stable zone of the train, where the train speed is 0. After 3 s it is defined as the motor zone of the train which starts to move with a given initial speed.

3 Dynamic responses of bridge deck and bed slab

To understand the dynamic responses of the bridge deck and the bed slab at different positions, two internodes at the ends of the model are used to simulate the boundary conditions, and the two internodes in the middle of the model is regarded as the calculation region (See Figure 3). The CRH2 train is adopted to pass through the six internodes at the speed of 200 km/h and the stiffness of elastic vibration-damping pad is 0.05 N/mm^3. The vertical peak accelerations of the bridge deck and the bed slab at different positions within the third internode are extracted (the vertical peak acceleration is the maximum acceleration of one node in the process of the train passing through the six internodes). Transverse and longitudinal coordinates of bridge deck within the third internode are shown in Figures 8(a) and (b). Figure 9 is the cloud chart of the vertical peak accelerations of bridge deck for each position within the third internode. The vertical peak accelerations of the bridge floor system can be divided into four regions in the transverse direction. They are the region beneath the track structure (the transverse position is from –2.15 to 0.65 m), the region with longitudinal beam supporting (the transverse position is from 0.65 to 7.2 m), the non-supporting region

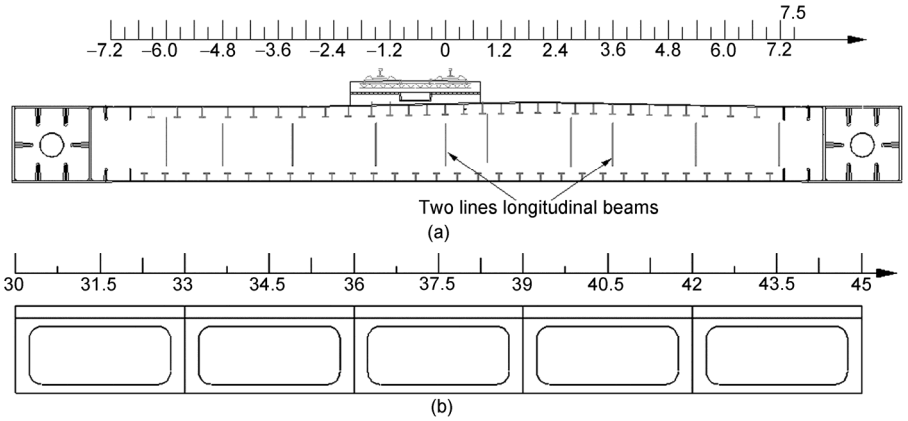

Figure 8 Bridge deck's coordinates (unit: m). (a) Transverse direction; (b) longitudinal direction.

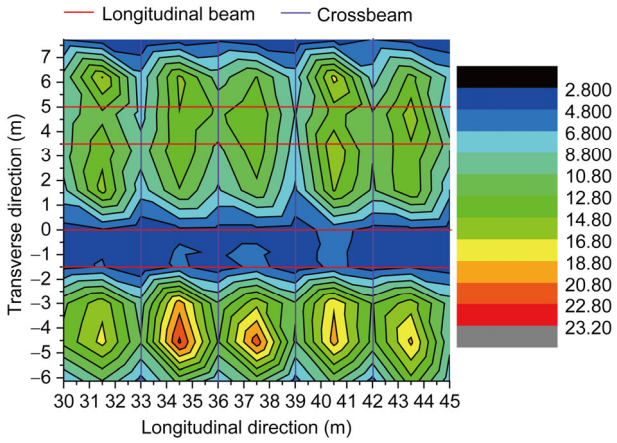

Figure 9 Cloud chart of the vertical peak accelerations of bridge deck within the third internode (with base plate).

(the transverse position is from −6.5 to −2.15 m) and the region near the bottom chord (the transverse position is from 7.2 to 8.05 m). Due to the supporting of the longitudinal beams and the co-stressing of the base plate, the vertical peak accelerations of the bridge deck beneath the track structure are relatively small. The vertical peak accelerations of the bridge deck near the bottom chord are also small due to the constraint function of the bottom chord. The non-supporting region of the bridge deck locating away from the longitudinal beams and bottom chord shows the maximum vertical peak acceleration. The distribution law of the vertical peak accelerations of the bridge deck in the longitudinal direction is that the smaller vertical peak accelerations are in the neighborhood of crossbeams while the largest are in the middle of two adjacent crossbeams. In summary, the bridge deck beneath the track structure within the third internode has the minimum vertical peak acceleration. The distribution law of vertical peak accelerations in other regions shows that it is divided into several lattice vibration regions by the longitudinal beams and crossbeams. The vertical peak acceleration is the largest in the middle of the lattices, while it is the smallest on the edge of the lattices. Therefore, when designing the orthotropic bridge floor system of the steel bridge with ballastless track, the multi-crossbeam floor system should be adopted in the longitudinal direction and the longitudinal beam should be set at a certain distance in the transverse direction to reduce the local vibration of bridge deck.

Figure 10(a) shows the vertical peak accelerations of the bridge deck in the transverse direction within the third internode. Within the 15 m internodes, the vertical peak accelerations of nodes in the transverse direction are extracted in every 1.5 m. It can be seen from the figure, due to sustaining the weight of the track structure and the railway longitudinal beam's supporting function, the vertical peak accelerations of the bridge deck beneath the track structure are all below 5 m/s^2. The vertical peak accelerations of the bridge deck in the central of the non-supporting region which is on the left side of the track structure have the maximum values, and the vertical peak accelerations are within the range of 10–22.5 m/s^2. The vertical peak accelerations in the region with longitudinal beam supporting are within the range of 7.5–15 m/s^2.

Figure 10(b) shows the vertical peak accelerations of bridge deck in the longitudinal direction within the third internode. For the bridge deck beneath the track structure and near the bottom chord (node *E*, *F*, *G*, *L*), their vertical peak accelerations are all less than 5 m/s^2, and are significantly lower than other locations. Be relative to the bridge deck on the right side of the track structure (node *I*, *J*, *K*), the bridge deck on the left side of the track structure (node *C*, *D*) has no setting of longitudinal beams. As a result, the acceleration response of the bridge deck on the left side of the track structure increases significantly. The longitudinal spacing of crossbeams is 3 m. The bridge deck located in the center of two adjacent crossbeams has much larger acceleration response than the bridge deck in the neighborhood of the crossbeams. Due to the restriction effect of the crossbeams, the acceleration response of bridge deck is the smallest at the position of crossbeams.

Figure 11 is the cloud chart of the vertical peak accelera-

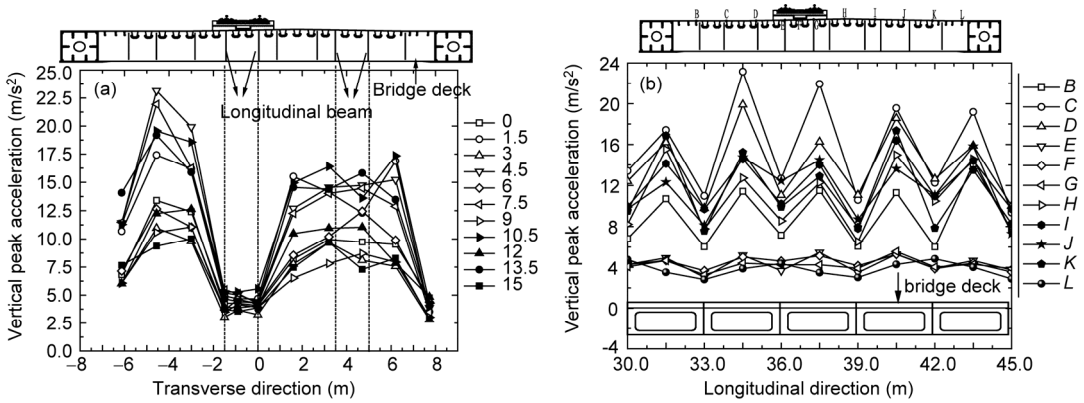

Figure 10 Vertical peak accelerations of the bridge deck. (a) Transverse direction; (b) longitudinal direction.

tions of the bed slab for each position within the third internode. The bed slab's width is 2.8 m and the length is 6 m. Figure 11 indicates that the vertical peak accelerations of the bed slab located on the edge of the joints and beneath the rail are larger than the other regions, and the maximum vertical acceleration is close to 6 m/s^2. The vertical peak accelerations of the joints (30, 36, 42 m) of the bed slab in the longitudinal direction are significantly larger than the center of the bed slab. The vertical peak accelerations on the left of joints (wheel sets existing side) are smaller than ones on the right of joints (wheel sets entry side). As the stiffness is discontinuous at the joints, there is a significantly impact action. As a result, the vertical peak accelerations of the joints of the bed slab are larger.

4 Influence of base plate and train speed

4.1 Influence of the base plate

The base plate is the supporting base of the ballastless track. Its main function is to fix the ballastless track's lower base deformation (subgrade settlement) before the construction and to achieve the ultra-high settings for the curve section [1]. The stiffness of the long-span plate truss cable-stayed bridge deck is large so that the ballastless track has the tendency of not setting up the concrete base plate, instead of setting up the lug boss on the bridge deck and the elastic vibration-damping pad between the bed slab and bridge deck. This section mainly discusses the necessity of setting up the base plate on the ballastless track laid on the long-span plate truss cable-stayed bridge from the aspect of dynamic responses of the bridge deck and the bed slab.

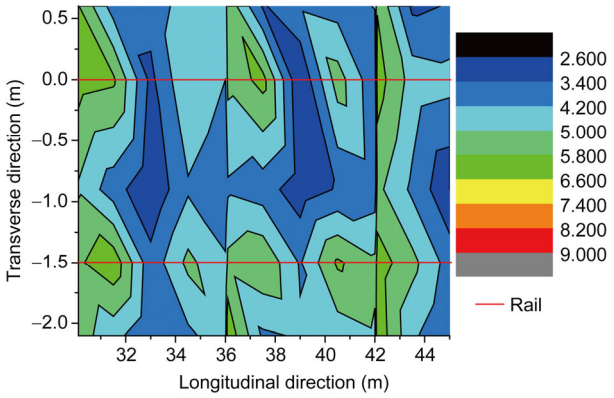

Figure 11 Cloud chart of the vertical peak accelerations of bed slab within the third internode (with base plate).

The CRH2 train is adopted during the research at the speed of 200 km/h. The stiffness of the elastic vibration-damping pad is 0.05 N/mm^3. Figures 12 and 9 are the cloud charts of the vertical peak accelerations of the bridge deck within the third internode without and with base plate respectively. After setting up the base plate, due to its participate in sharing forces, the bridge deck beneath the base plate has much smaller vertical peak accelerations than the one having no base plate. The region between two lines longitudinal beams (shown in Figure 8(a)) is also affected more apparently by the base plate and the vertical acceleration response of the bridge deck in this region decrease obviously after setting up the base plate. Because the lower chord shows more constraint effect to bridge deck in this region, the base plate has less effect on the vertical acceleration response of the bridge deck near the bottom chord.

Figure 13 is the comparison of the vertical peak accelerations of bridge deck at the transverse coordinates of –0.9, 1.6 and 7.73 m within the third internode, with and without the base plate, respectively. As the figure, the affection on the vertical peak accelerations of the bridge deck by the base plate is less at the transverse coordinates of 7.73 m (region near the bottom chord). However, the vertical peak accelerations at the transverse coordinates of –0.9 m (the region beneath the track structure) and 1.6 m (the region between the two lines longitudinal beams) show significant differences with and without setting up the base plate. After setting up the base plate, the maximum reductions of vertical peak accelerations are 5.1 and 7.6 m/s^2 respectively.

Figures 14 and 11 are the cloud charts of the vertical peak accelerations of the bed slab within the third internode,

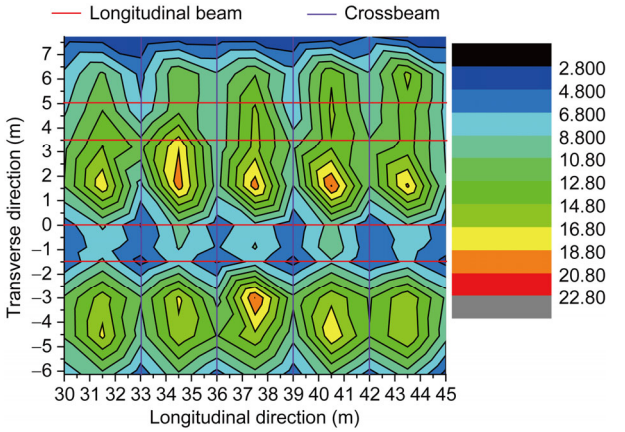

Figure 12 Cloud chart of the vertical peak accelerations of bridge deck (without base plate).

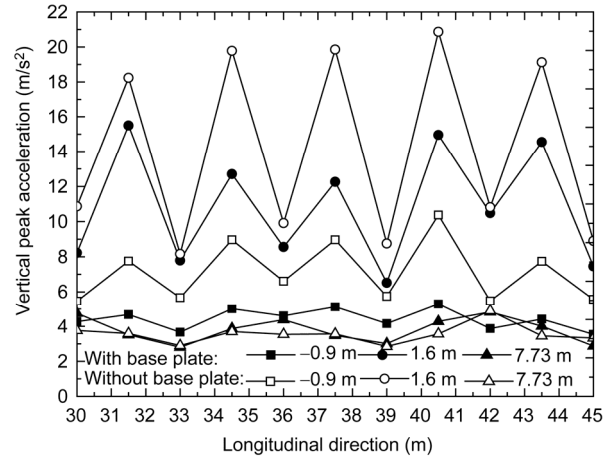

Figure 13 Comparison of the vertical peak accelerations of bridge deck.

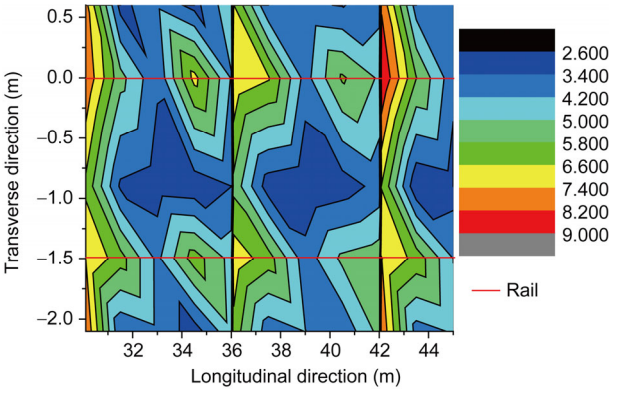

Figure 14 Cloud chart of the vertical peak accelerations of bed slab (without base plate).

without and with setting up the base plate, respectively. It can be seen from the figures, whether to set up the base plate or not, has little effect on the vertical peak accelerations in the central part of the bed slab, but the affection on the vertical peak accelerations of the joints of bed slab is obvious.

In summary, the setting of base plate significantly reduces the acceleration responses of the bridge deck beneath the track structure and between the two lines longitudinal beams, and reduces the acceleration responses of the joints of the bed slab as well. It is necessary to set up the base plate on the ballastless track laid on the long-span plate truss cable-stayed bridge simply from the aspect of reducing the dynamic responses of the bridge deck and the bed slab.

4.2 Influence of train speed

When the train passes through the six internodes at the speed of V, the change of V will cause the change of dynamic responses of the bridge deck and bed slab. This section focuses on the effect of various speeds on the maximum vertical accelerations and displacements of the bed slab and the bridge deck beneath the track structure. The stiffness of the elastic vibration-damping pad used in calculation is 0.05 N/mm^3. ICE3 train runs with the speeds of 200, 240, 280, 300 and 350 km/h.

Figures 15 and 16 respectively show the influence of the train speed on the maximum vertical accelerations and displacements of the bed slab and the bridge deck beneath the track structure. The figures show that the maximum vertical accelerations of the bed slab increase with the increasing of train speed while the change law of the bridge deck beneath the track structure is not very clear. As the bed slab bears the train load directly, increasing of the train speed amplifies the impacting action of the train load on the bed slab. So when the speed changes from 200 to 350 km/h, the maximum vertical acceleration of the bed slab increases obviously. The train speed has limited influence on the maximum vertical displacements of the bed slab and bridge deck beneath the track structure.

The bed slab is an ordinary reinforced concrete structure, which is applied prestress in both the longitudinal and transverse directions. Beneath the bed slab, the elastic vibration-damping pad with lower stiffness is set up. All of

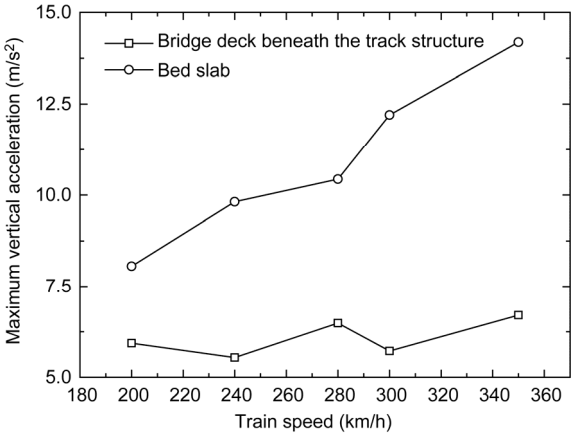

Figure 15 Influence of train speeds on the maximum vertical acceleration.

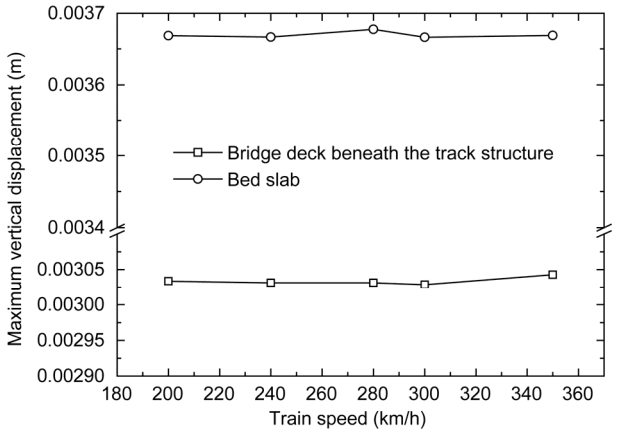

Figure 16 Influence of train speeds on the maximum vertical displacement.

these make the supporting ability of bed slab weak and the loading condition complicated. With the change of train speed, the dynamic response of the bed slab also experiences certain changes. Figures 17(a)–(e) are cloud charts of the vertical peak accelerations of the bed slab within the third internode under different train speeds. The figures show that the maximum vertical acceleration of the bed slab appears in the region beneath the rail and the joints of the bed slab. With the increasing of the train speed, the range of the maximum vertical acceleration expands around, which shows that the dynamic response of the bed slab is getting larger. The position of the maximum vertical acceleration is at the first piece of bed slab within the third internode when the speed is 350 km/h.

5 Influence of the stiffness of elastic vibration-damping pad

Elastic vibration-damping pad is an important component of a double-block ballastless track. Its main function is to transfer and bear force and reduce noise and vibration. It

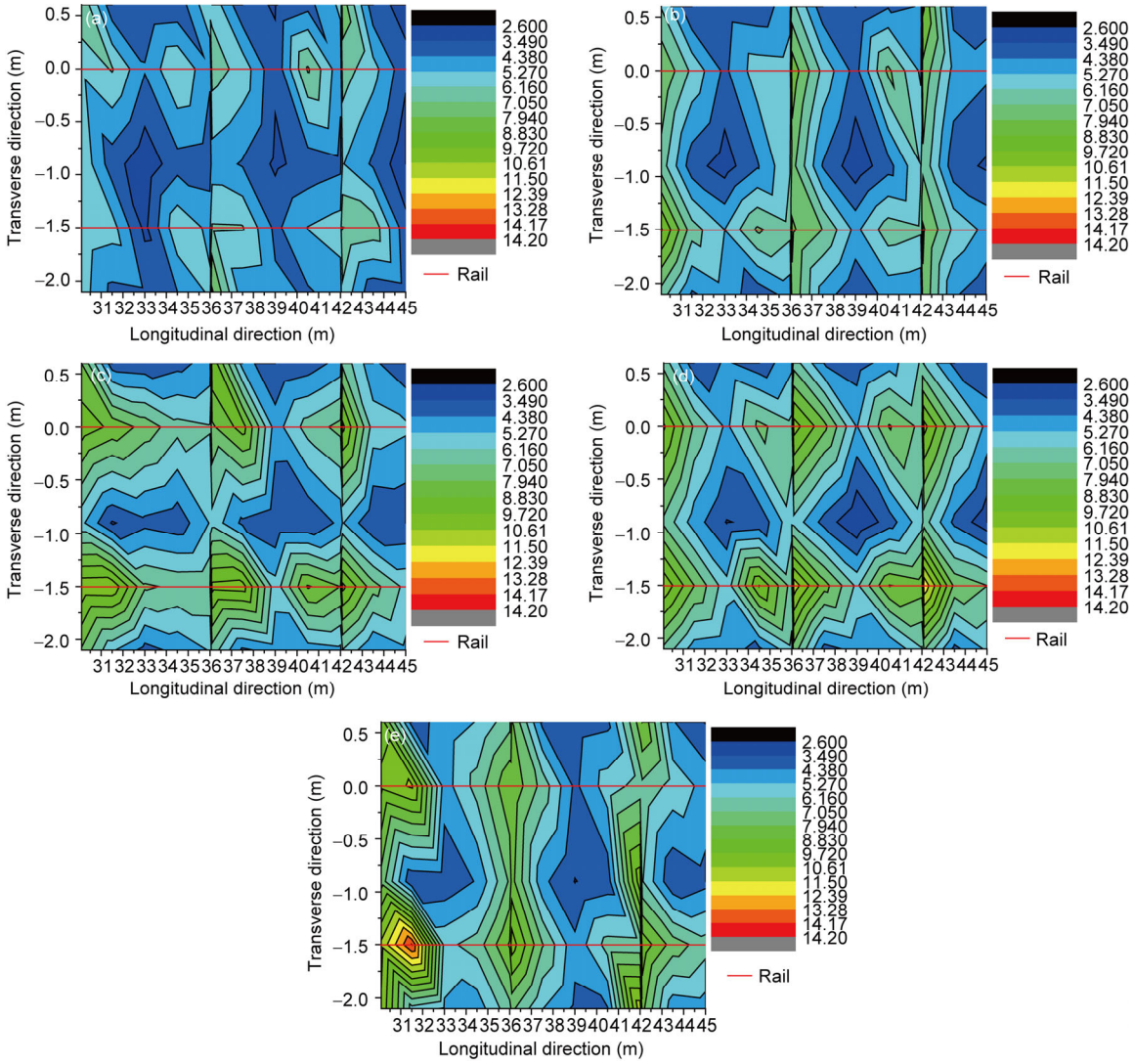

Figure 17 Cloud chart of the vertical peak accelerations of bed slab under different train speeds. (a) Train speed: 200 km/h; (b) train speed: 240 km/h; (c) train speed: 280 km/h; (d) train speed: 300 km/h; (e) train speed: 350 km/h.

fully supports the bed slab and eliminates the gap between the bed slab and the base plate. It bears the vertical and horizontal forces coming from the bed slab and decentralizes the action of the train loads by transferring forces to the base plate and the limit device. It reduces the vibration of the bed slab and the bridge deck as well as the noise induced by the train passing through the bridge.

To compare the effect of vibration reduction of different stiffness of elastic vibration-damping pad, three common stiffness of elastic vibration-damping pad 0.05, 0.1 and 0.15 N/mm^3 are selected. The CRH2 train is adopted at the speed of 200 km/h. At the location of the bed slab and the bridge deck beneath the track structure where the maximum vertical accelerations appear within the third internode, the time history of the acceleration is extracted to process the time domain analysis and spectrum analysis.

The maximum vertical accelerations of the bed slab and bridge deck beneath the track structure within the third internode are shown in Table 6, and the vibration acceleration level is calculated with reference to the international standard [22].

It can be seen from the table, when the stiffness of elastic vibration-damping pad is 0.05 N/mm^3, the bridge deck beneath the track structure and the bed slab have their maximum vertical accelerations of 5.57 and 6.37 m/s^2 respectively. For the two cases that the stiffness of elastic vibration-damping pads are 0.05 and 0.10 N/mm^3, the maximum vertical accelerations of the bridge deck have a large difference and discrepancy of the maximum vibration acceleration level is 1.2 dB. The discrepancy of the maximum vertical acceleration of the bed slab is relatively limited. For the two cases that the stiffness of elastic vibration-damping pads are 0.05 and 0.15 N/mm^3, the maximum vertical acceleration of the bridge deck has a limited difference while the difference of the maximum vertical accelerations of the bed slab is quite large and the discrepancy of the maximum vibration acceleration level is 2.4 dB.

Increasing the stiffness of the elastic vibration-damping pad, the maximum vertical acceleration of the center of train's gravity is reduced significantly. But for all the three cases, the maximum vertical accelerations of the center of train's gravity are all small. From the aspect of reducing the vertical acceleration response of the bridge deck beneath the track structure and the bed slab, the elastic vibration-damping pad with stiffness of 0.05 N/mm^3 has a relatively good damping effect.

In order to further compare the characteristics of frequency-domain of different elastic vibration-damping pads and the effects of vibration reduction in different frequency bands, spectrum analysis is introduced to analyze the vertical accelerations at the position where the bridge deck and the bed slab have their maximum vertical accelerations under the three stiffness of elastic vibration-damping pads. Based on the spectrum analysis, the vibration acceleration level of 1/3 octave center frequency is calculated.

Figures 18(a)–(c) are the time history and the power spectrum of acceleration with the Fast Fourier Transform (FFT) at the position where the bridge deck and the bed slab have their maximum vertical accelerations under the three stiffness of elastic vibration-damping pads. These figures show that the predominant frequencies of vertical vibration of the bridge deck and the bed slab are mainly concentrated on the low frequency portion (1–20 Hz) and high frequency part (100 Hz or more), while the amount of medium frequency (20–100 Hz) is quite small.

Figure 19 is the vibration acceleration level of 1/3 octave center frequency of the bridge deck and bed slab. The figure shows that in the range of 1–5 Hz the elastic vibration-damping pad with larger stiffness causes lesser vibration of the bridge deck. Within the scope of 5–20 Hz, elastic vibration-damping pad with low stiffness has the better effect of vibration reduction to the bridge deck vibration. For the range of 20–80 Hz, elastic vibration-damping pad with larger stiffness has better effect of vibration reduction to the bridge deck vibration. Within the high frequencies (80–400 Hz), the stiffness of elastic vibration-damping pad which is 0.05 N/mm^3 shows a relatively good effect of vibration reduction. Based on Figure 19, elastic vibration-damping pad with low stiffness has a relatively good effect of vibration reduction to the bed slab within the entire frequency band and shows more obvious effect of vibration reduction in low frequency band and high frequency band. In the low frequency and medium frequency band, elastic vibration-damping pad with the stiffness of 0.1 N/mm^3 has the better effect of vibration reduction than that of 0.15 N/mm^3. In the high frequency band, elastic vibration-damping pads with stiffness of 0.1 and 0.15 N/mm^3 have the same effect of vibration reduction.

Spectrum analysis of the vertical accelerations indicates that the predominant frequency of the bridge deck is mainly distributed into the low frequency part (11.9 Hz) and high frequency part (180 Hz or more), and the high frequency component takes more portion. It indicates that the elastic vibration-damping pad with low stiffness should be adopted.

Table 6 Dynamic responses of different stiffness of elastic vibration-damping pad

Stiffness of elastic vibration-damping pad (N/mm^3)	Bridge deck		Bed slab		Train gravity's maximum vertical acceleration (m/s^2)
	Maximum vertical acceleration (m/s^2)	Maximum vibration acceleration level (dB)	Maximum vertical acceleration (m/s^2)	Maximum vibration acceleration level (dB)	
0.05	5.57	134.91	6.37	136.09	0.11
0.10	6.43	136.16	6.39	136.11	0.053
0.15	5.87	135.37	8.40	138.49	0.044

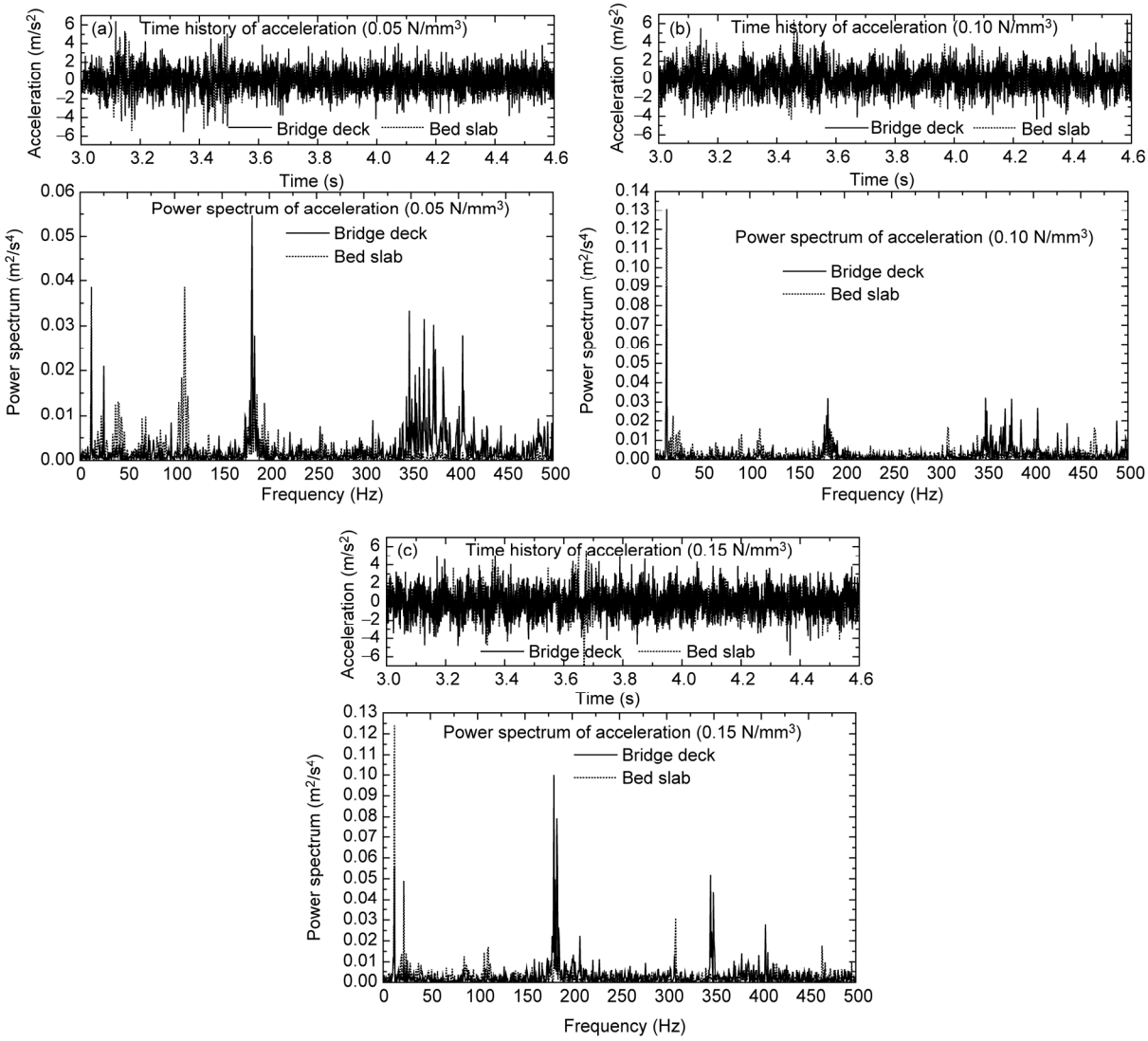

Figure 18 Time history and power spectrum of acceleration of bridge deck and bed slab under the different stiffness of elastic vibration-damping pads. (a) Stiffness of elastic vibration-damping pad: 0.05 N/mm^3; (b) stiffness of elastic vibration-damping pad: 0.1 N/mm^3; (c) stiffness of elastic vibration-damping pad: 0.15 N/mm^3.

The bed slab's predominant frequency is mainly distributed in the low frequency part (11.9 Hz), and elastic vibration-damping pad with the stiffness of 0.05 N/mm^3 has a relatively good effect of vibration reduction to bed slab.

Combining the results of the time-domain analysis and spectral analysis, the stiffness of the elastic vibration-damping pad should be preferred to 0.05 N/mm^3 just from the aspect of decreasing the vertical accelerations of the bridge deck and the bed slab.

6 Conclusions

By simulating the dynamic process for a single train passing through the six sections of long-span plate-truss cable-stayed bridge, this paper discusses the distribution law of the dynamic responses of the bridge deck and the bed slab

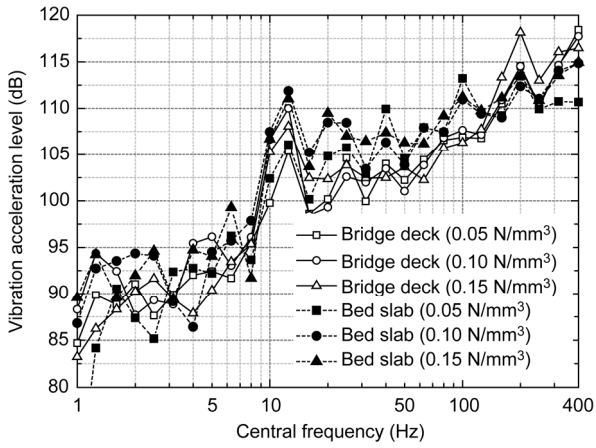

Figure 19 Comparison of vibration acceleration level of 1/3 octave center frequency of bridge deck beneath the track structure and bed slab.

within the third internode. Some conclusions are drawn as follows.

(1) When designing the bridge floor system with the ballastless track, the multi-crossbeam floor system should be adopted in the longitudinal direction and the longitudinal beam should be set at a certain distance in the transverse direction in order to reduce the local vibration of bridge deck.

(2) According to the influence of the base plate on the dynamic responses, it is necessary to set up the base plate for the ballastless track laid on the long-span plate truss cable-stayed bridge from the aspect of reducing the dynamic responses of the bridge deck and bed slab.

(3) The maximum vertical acceleration of the bed slab increases with the increasing of train speed. The train speed has limited influence on the maximum vertical displacements of the bed slab and bridge deck beneath the track structure.

(4) Comparison of the influence of three different stiffness of elastic vibration-damping pads on the dynamic responses of the bridge deck and the bed slab is made. It is shown that the stiffness of the elastic vibration-damping pad should be preferred to choose 0.05 N/mm^3 rather than 0.10 and 0.15 N/mm^3, just in view of decreasing the vertical accelerations of the bridge deck and the bed slab.

This work was supported by the National Natural Science Foundation of China (Grant No. NNSF-U1334201), the National Basic Research Program of China ("973" Project) (Grant No. 2013CB036206), and the Sichuan Province Youth Science and Technology Innovation Team (Grant No. 2015TD0004).

1 He H W. Ballastless Track Technology (in Chinese). Beijing: China Railway Publishing House, 2005. 1–5
2 Zhai W, Xia H, Cai C, et al. High-speed train–track–bridge dynamic interactions–Part I: Theoretical model and numerical simulation. Int J Rail Transportation, 2013, 1: 3–24
3 Zhai W, Wang S, Zhang N, et al. High-speed train-track-bridge dynamic interactions–Part II: Experimental validation and engineering application. Int J Rail Transportation, 2013, 1: 5–41
Timoshenko S. On the forced vibrations of bridges. Philos Mag Ser, 1922, 43: 1018–1019
4 Mise K, Kunii S. A theory for the forced vibration of a railway bridge under the action of moving loads. Q J Mech Appl Math, 1956, 9: 195–206
5 Frýba L. Dynamics of Railway Bridges. London: Thomas Telford, 1996
6 Arvidsson T, Karoumi R. Train-bridge interaction–a review and discussion of key model parameters. Int J Rail Transportation, 2014, 2: 147–186
7 Zhai W M, Cai C B. Train/track/bridge dynamic interactions: imulation and applications. Veh Syst Dyn, 2002, 37: 653–665
8 Zhai W M, Cai C B, Wang K Y. Numerical simulation and field experiment of high-speed train-track-bridge system dynamics. Veh Syst Dyn, 2004, 47: 677–686
9 Cheng Y S, Au F T K, Cheung Y K. Vibration of railway bridges under a moving train by using bridge-track-vehicle element. Eng Struct, 2001, 23: 1597–1606
10 Zhang N, Zhou S, Xia H, et al. Evaluation of vehicle-track-bridge interacted system for the continuous CRTS-II non-ballast track slab. Sci China Tech Sci, 2014, 57: 1895–1901
11 Biondi B, Muscolino G, Sofi A. A substructure approach for dynamic analysis of train-track-bridge system. Comput Struct. 2005; 83: 2271–2281
12 Zhu S Y, Fu Q, Cai C B, et al. Damage evolution and dynamic response of cement asphalt mortar layer of slab track under vehicle dynamic load. Sci China Tech Sci, 2014, 57: 1883–1894
13 Lou P, Yu Z W, Au FTK. Rail–bridge coupling element of unequal lengths for analyzing train–track–bridge interaction systems. Appl Math Model, 2012, 36: 1395–1414
14 Wu Y S, Yang Y B, Yau J D. Three-dimensional analysis of train-rail-bridge interaction problems. Veh Syst Dyn, 2001, 36: 1–35
15 Guo W W, Xia H, De Roeck G, et al. Integral model for train-track-bridge interaction on the Sesia viaduct: Dynamic simulation and critical assessment. Comput Struct, 2012, 112-113: 205–216
16 Livermore software technology corp. Ls-dyna Keyword User's Manual. California, 2007
17 Fan J J. Modern Railway Track (in Chinese). 2nd eds. Beijing: China Railway Publishing House, 2004
18 Chen G, Zhai W M. A new wheel/rail spatially dynamic coupling model and its verification. Veh Syst Dyn, 2004, 41: 301–322
19 Li Y L, Qiang S Z, Liao H L, et al. Dynamics of wind–rail vehicle-bridge systems. J Wind Eng Ind Aerod, 2005, 93: 483–507
20 Klasztorny M, Szurgott P. Modeling and simulation of bridge-track-train systems at high service velocities with LS-DYNA. In: 12th International LS-DYNA Users Conference, Detroit, 2012
21 Ministry of Environmental Protection of China. GB10071-88, Measurement Method of Environmental Vibration of Urban Area. Beijing: China Standard Publishing House, 1989